Surface-structure dependence of water-related adsorbates on platinum

Badan, C.

Chapter 4

How well Does Pt(211) Represent Pt[n(111)x(100)] Surfaces in Adsorption/Desorption?

4.1 Abstract

We have investigated to what extent Pt(211) is representative for Pt[n(111)x(100)] surfaces in adsorption/desorption behavior of water, hydrogen, and oxygen through temperature programmed desorption. In contrast to surfaces with n > 3, H_2O adsorbs to Pt(211) in a crystalline fashion far below the usual crystallization temperature of amorphous solid water. For D_2, we find that desorption from (100) steps is independent of terrace length for n ≥ 3, but desorption from the neighboring (111) terraces varies. Larger terraces result in larger variations in binding energies as a consequence of decreasing proximity of adsorption sites to the step edge. For O_2, we observe enhanced dissociation on Pt(211) resulting in a much larger maximum O-coverage than surfaces with n > 3. The TPD characteristics suggest formation of 1-

dimensional PtO_2 structures, which are only formed for n=3 with this (100) step type. Hence, Pt(211) can by no means be considered representative of Pt(111) terraces truncated by (100) steps. Our results stress that great caution is required when extrapolating results from theoretical studies based on this smallest unit cell containing the (100) step edge to catalysis by actual particles.

Based on: Badan, C.; Koper, M. T. M.; Juurlink, L. B. F., J. Phys. Chem. C 2015, 119, 13551-13560.

4.2 Introduction

As an exceptional catalyst for industrial, automotive and fuel cell catalysis, platinum has been the subject of numerous theoretical and experimental studies. Because of its multiple uses, global production and consumption of platinum has increased intensely in the last 30 years although it remains one of the most expensive precious metals[1]. To reduce costs, Pt either needs to be replaced by an alternative, less expensive catalyst material or its catalytic activity needs to be enhanced to lower the required volume while achieving the same kinetic rates. For the latter, it is vital to improve our understanding of structure-activity and structure-selectivity relations[2]. One way to elucidate the influence of local surface structure to chemical reactions is to compare reactivity of various well-defined, high and low-Miller-index single-crystal catalyst surfaces under well-controlled conditions.

Prototypical surface science and gas-surface dynamics studies for Pt involve CO, H_2, O_2 or H_2O. In this paper, we focus on the adsorption and desorption of the latter three molecules. These three molecules prove to be excellent probes as they represent for Pt(111) and its vicinal surfaces both non-dissociative (H_2O[3, 4]) and dissociative adsorption (O_2[5, 6] H_2[7, 8]) with varying ranges of activation barriers and either directly dissociating (H_2[9, 10]) or passing through well-defined intermediate states (O_2[11, 12]). In addition, they yield adsorbates with both weak (H) and strong lateral interactions (O), also leading to large variations in maximum surface coverage. For the infinite (111) terrace, the maximum coverage is 1 H/Pt[7] while for O it is 0.25 O/Pt atom[13] using, respectively, H_2 and O_2 as gaseous reactants. Beyond attractive or repulsive interaction, H_2O tends to form long-range networks on Pt(111)[14].

It has been shown that the geometry of the step type may have varying effects on adsorption, ranging from inducing hydrophobic vs hydrophilic behavior for co-adsorbed D and H_2O[15] and preferring O vs OH adsorption at the step edge for co-adsorbed O and H_2O[16]. We now investigate whether *terrace width* is a second parameter that must be explicitly treated in theoretical modelling of platinum catalysis. Here, we use the same three probe molecules and temperature programmed desorption (TPD) as our main technique. In particular, we focus on differences observed for Pt surfaces containing the (100) step edge. The (211) surface, also indicated as [3(111)x(100)] in the van Hove-Somorjai notation[17], is often taken as the reference for (100) step edge effects in DFT studies comparing binding energies and activation barriers to dissociation on (111) (e.g. refs[18–20]). We will show that the (211) surface shows significant differences from [n(111)x(100)] surfaces for $n > 3$ and conclude that (211) is not a surface that can be chosen to generally represent structural effects for (100) step edges.

4.3 Experimental

Experiments are carried out using a custom-built vacuum (UHV) surface science chamber which is primarily used for LEED and TPD studies. The system and our standard procedures have been described elsewhere[21, 22]. This system has a base pressure of 5×10^{-11} mbar. The chamber is equipped with two quadrupole mass spectrometers (QMS). One QMS (Baltzers, Prisma 200) protrudes into the main chamber and is mainly used for residual gas analysis (RGA). The other QMS (Baltzers QMA 400) is kept in a differentially pumped canister that connects to the main UHV chamber via a circular spot with a radius of 2.5 mm. The crystal is positioned 2 mm from the face of the sample during TPD studies. The apparatus also contains, amongst others, a sputter gun (Perkin Elmer 20-045) and LEED optics (VG RVL 900). Lastly, it contains three directional dosers which provide localized effusive dosing onto the sample. For the experiments described in this paper, single-crystals, (Surface Preparation Laboratory, Zaandam, the Netherlands) are 1 or 2 mm thick and 10 mm in diameter. The sample can be cooled to ∼95 K by pouring LN2 into the cryostats reservoir. The crystals are heated radiatively by a filament (Osram, 250 W) mounted behind the sample. Samples can be also heated by electron bombardment using a positive voltage on the crystal assembly while the filament is grounded. For the crystals, temperature is measured by a type-K thermocouple laser welded to the top edge of the samples. For temperature control, we use a PID controller (Eurotherm 2416) from which the thermocouple is electrically decoupled.

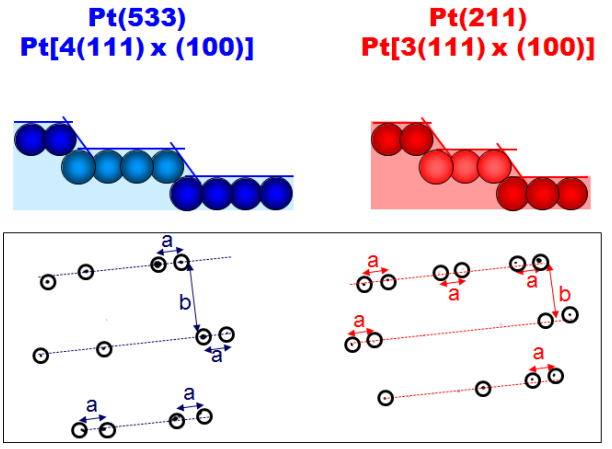

Figure 4.1: Schematic side views (top) and inverted LEED patterns (bottom) of clean Pt(533) (left) and Pt(211) (right).

Crystals are cleaned by repetitive sputtering-annealing cycles. We sputter using Ar^+ (Messer, 5.0) at 500 V and 2 μA for 20 minutes and anneal at 900 K in an O_2 atmosphere (5×10^{-8} mbar) for 5 minutes. Finally we anneal the crystal at 1200 K for 5 minutes. LEED was periodically used to check surface order. The top panel of figure 4.1 shows schematic side view representations of the Pt(533) and Pt(211) that consists of 4 and 3 atom wide (111) terraces with (100) steps, respectively. The bottom panel shows the LEED spots from color-inverted photos taken of the LEED diffraction patterns after cleaning these surfaces. From these images, we deduce spot row spacing to spot splitting ratios (indicated by the dotted lines and double-headed arrows) of 3.24 for Pt(533) and 2.38 for Pt(211). These values correspond well to the literature values of 3.28 and 2.45[17].

Water (Millipore, 18.2Ω) was dosed onto our Pt crystals using a custom-built 10 mm diameter capillary array doser at a distance large enough to ensure a uniform flux across the entire cleaned surface[23]. The water was degassed by multiple freeze-pump-thaw cycles and backfilled with 1.1 bar He (6N, Air Products) prior to experiments. Water, D_2 (Linde 2.8) and O_2 (Messer, 5.0) are dosed directly onto the surface with $T_s \leq 100$ K. During dosing all filaments were switched off to minimize contamination by H atoms. The gases were generally dosed onto the crystal for different durations at a fixed pressure. The pressure is determined by an uncalibrated cold cathode gauge. For all TPD experiments, the sample was heated with ~ 0.9 K s^{-1} to a temperature well above completion of desorption. Subsequently, the sample is annealed to 1200 K again for 5 minutes. For experiments involving D_2, m/z = 2 (H_2), 3 (HD) and 4 (D_2) were monitored. We found no significant desorption of H_2 and HD. Baseline correction and fitting procedures are described in detail elsewhere[16, 24].

To determine the absolute coverages for H_2O, and O_2 we used flat Pt(111) as reference. In chapter 5 and 7, we explain our reference method in greater detail. For deuterium, the maximum integrated TPD signal is set to a saturation value of 0.9 ± 0.05 ML as reported previously[25]. To obtain kinetic parameters, we have attempted to apply several methods. A complete analysis[26] for D_2, H_2O, and O_2 unfortunately yields unreliable results as trailing edges show significant overlap. Minor variations in the background subtraction affect the onset for the individual TPD features too strongly to obtain consistent desorption energies and frequency factors using a leading edge analysis[27]. The inversion-optimization method[28] can only be applied to a spectrum of multiple peaks when those represent a single desorption order. This seems not to be the case in our spectra. Our attempts to separate the individual peaks and analyze them individually did not result in a determination of kinetic parameters with a significant degree of accuracy.

4.4 Results and discussion

4.4.1 Water

Figure 4.2 shows TPD spectra of H_2O desorbing from the clean Pt(211) surface. Water desorption is characterized by two main features. The maximum rate of desorption for the higher temperature peak appears at ∼193 K. For the lower temperature peak, it shifts from 150 to 165K for these coverages. The onset of desorption appears at ∼140 K. We do not observe an explicit desorption peak appearing between 170 and 180 K as is generally observed for Pt[n(111)(100)] surfaces with n≥4[29]. Based on previous studies, the low and high temperature desorption peaks may be attributed respectively to desorption of water molecules from the second or consecutive water layers[16, 29, 30], and molecules in contact with the bare Pt surface, in particular the (100) step sites[16, 29]. In comparison to other Pt surfaces with the same step type but wider terraces, we find significant differences that deserve a detailed comparison.

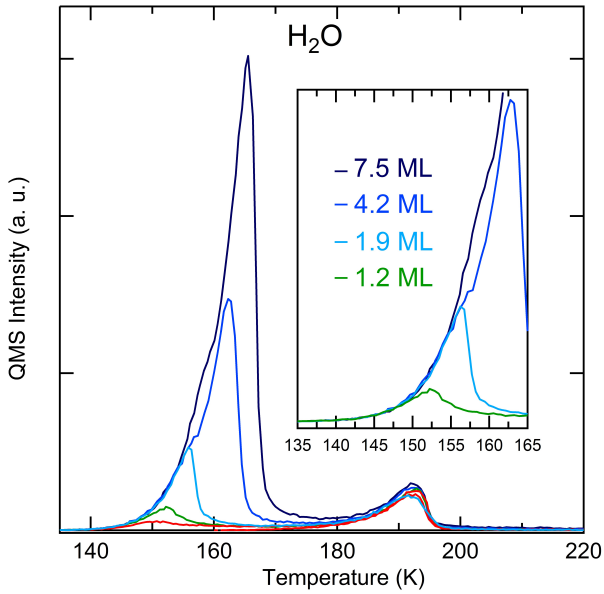

Figure 4.2: TPD spectra of various amounts of H_2O desorbing from clean Pt(211) at 0.9 K s^{-1}.

The multilayer desorption peak appears only after saturation of the high temperature peak. Although it exhibits characteristics of 0^{th}-order desorption kinetics, the inset shows that the second and consecutive water layers are not equi-

valent. For coverages between 1 and 2 ML, leading edges overlap perfectly. For coverages larger than 2 ML, leading edges also overlap but clearly show a steeper onset than for the second water layer. The latter TPD spectra also exhibit the characteristic deflection at ∼158 K in desorption rate that indicates crystallization of amorphous solid water (ASW) to crystalline ice (CI) during the temperature ramp[31–33]. We find no evidence of a crystalline layer from LEED measurements.

Finally, the leading edges for the lower temperature desorption of coverages between 1 and 2 ML align perfectly with the desorption rate for > 2 ML after crystallization. From these results, we conclude that the second layer of H_2O on Pt(211) is of a crystalline nature prior to the onset of desorption. As it seems unlikely that a crystalline layer forms on top of a disordered layer, the water layer directly in contact with the Pt(211) substrate, which desorbs around 200 K, is expected to be crystalline at the onset of desorption of the second layer. Although our current data does not exclude that crystallization occurred during the temperature ramp between 100 and 140 K, we see no reason why this would involve only the first two layers and leave thicker layers as ASW to be crystallized only around 158 K. Hence, we believe that the surface structure of Pt(211) induces crystalline water growth at 100 K already with the second water layer also being of crystalline. The third and consecutive layers grow at 100 K as ASW on top of this crystalline structure. Although similar water growth has been observed, e.g. for ASW growth on top of a single CI layer on Pt(111)[34–37], we believe the observed behavior involving two crystalline water layers prior to ASW growth at such a low surface temperature is unique. We have attempted to find additional diffraction spots using LEED for various water coverages but found none.

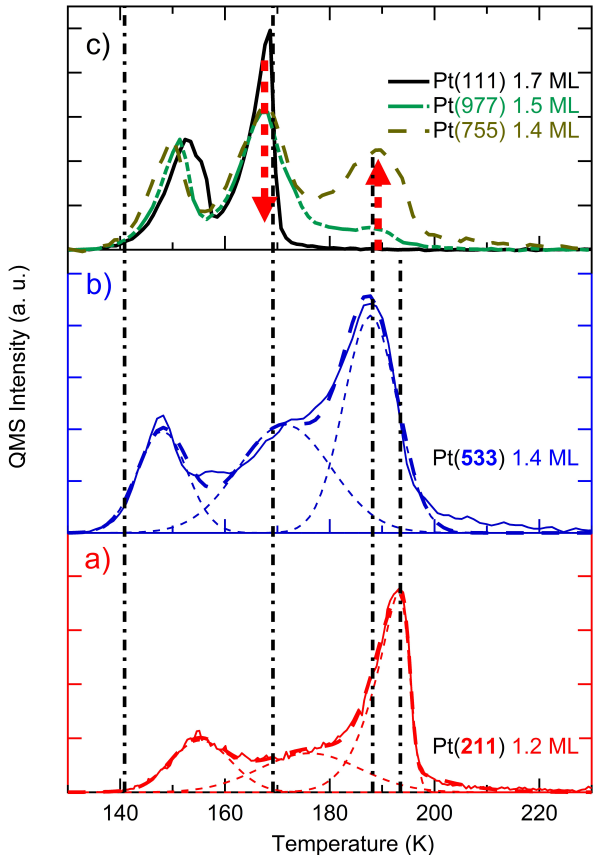

Figure 4.3: Comparison of H_2O TPD spectra for a) Pt(211) b) Pt(533) and c) Pt(755), (977) and (111)[29]. The dashed-dotted vertical lines guide the eye. Arrows indicate peak progression upon increasing step density.

Figure 4.3 compares TPD spectra of H_2O desorbing from Pt(533) and Pt(211), middle and bottom sections, respectively. In the top panel, we also show our TPD spectra of H_2O from Pt(111), Pt(977) and Pt(755)[29]. The dotted lines in the data for Pt(533) and Pt(211) represent the three desorption peaks from a fitting procedure on the basis of three modified Gaussian functions to model desorption of water in different environments. These components are used for qualitative comparison only and we assign no value to it other than that this simple procedure reproduces the actual spectra quite well. Similar to Pt(211), Pt(533) gives rise to two distinct water desorption features. However, here the high temperature peak shows a maximum desorption rate at 188 K. This is the same temperature

observed for the maximum desorption rate of (100) step-bound water on Pt(755) and Pt(977). For Pt(533), a shoulder appears at ∼170 K[16]. By comparison to the other stepped surfaces and Pt(111), this was previously associated with desorption of water bound on (111) terrace sites[29]. The onset of the multilayer desorption feature and the step peak from Pt(533), Pt(977) and Pt(755) appear at lower temperatures as compared to Pt(211) (dashed-dotted vertical lines). On the basis of these results, we suggest that there is a discontinuity in water adsorption behavior to Pt[n(111)x(100)] surfaces that appears when reducing the terrace width below n=4.

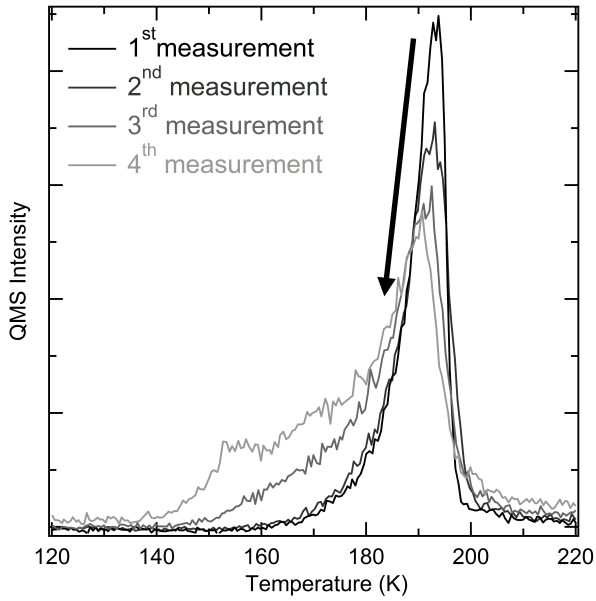

Figure 4.4: TPD spectra of nearly identical H_2O coverages desorbing from Pt(211). After each TPD measurement the sample was cooled, without heating to the temperature where oxygen starts desorbing.

We noted that the TPD data in figure 4.2 for Pt(211) suggest a crystalline nature for the first two layers (see chapter 5). The considerably higher desorption temperature for the water layer in contact with the Pt surface as compared to surfaces with wider terraces may result from an additional stabilization for water bound to the (100) step edge[29]. As the terraces are very narrow, one can imagine that step-bound water interacts not only through H-bonding along the step edge[38, 39], but also directly with water bound to neighboring steps. On the other hand, one may also consider the upward temperature shift to reflect (par-

tial) dissociation of water at step edge. Fajin et al. recently calculated binding energies for individual H_2O molecules and the OH_{ads} + H_{ads} products to Pt(211) using density function theory (DFT)[40]. Although dissociation was found to be exothermic, the activation energy was higher than the adsorption energy (0.66 eV and 0.41 eV, respectively). Hence, they concluded that dissociation was not to be expected. Although our current data is not conclusive, we have reason not to discard dissociation entirely. First, although our Pt(211) surfaces shows all LEED characteristics of a well-behaved step structure with mono-atomic high steps, kinks in these steps are very likely present. Dissociation at kinks and at steps for water clusters may well compete with desorption during the temperature ramp, as was found in DFT calculations for isolated molecules on Pt(321)[41]. Second, figure 4.4 shows small but continuous changes in TPD spectra for repeated water doses with consecutive temperature ramps when the surface is not annealed at temperatures above the associative desorption temperature of O_2 in between water doses. We observe that after each experiment, the intensity of the step peak drops. This may suggest that the first water layer indeed dissociates in part producing some H and OH groups. These products may desorb recombinatively as H_2O leaving a clean surface, but this would not explain changes in consecutive TPD spectra. On the other hand, OH groups may also recombinatively desorb as H_2O leaving O_{ads} on the surface. This may explain observed changes in consecutive experiments.

4.4.2 Deuterium

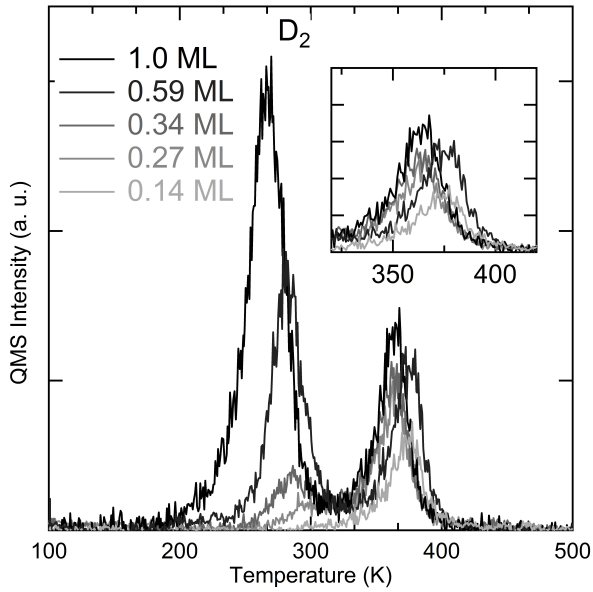

Figure 4.5: D_2 TPD spectra for Pt(211) for various initial coverages. The inset shows desorption from the (100) steps in greater detail.

In figure 4.5 we show TPD spectra for various amounts of D_2 associatively desorbing from Pt(211). For low initial coverages, a high temperature desorption peak saturates at 374 K. After saturation, a second peak appears, its maximum shifting continuously from 315 to 277 K. A comparison to previous studies suggests that the high temperature peak originates from recombinative desorption occurring at (100) step sites, while the low temperature peak results from desorption from (111) terrace sites[16, 25, 42, 43]. For desorption from terraces, trailing edges overlap mostly. This behavior characterizes second-order desorption kinetics and may be expected from associative desorption from a uniform surface with no dependence of binding energy on surface coverage. For desorption from the (100) steps, the inset of figure 4.5 shows more detail although it does not allow us to draw conclusions regarding the kinetic order of desorption.

In figure 4.6 we compare TPD spectra of the highest obtained D_{ads} coverage on Pt(533) and Pt(211), on the top and bottom panels, respectively. The two spectra consist of two peaks at saturation, both of which are reproduced rather accurately using Gaussian line shape fits. On Pt(533), the step and terrace desorption peaks saturate at 376 K and 264 K. In contrast to desorption of H_2O, for

D_2 the (100) steps of Pt(211) and Pt(533) give rise to maximum desorption rates at nearly identical temperatures, although the desorption feature for the (100) step on Pt(533) is slightly broader. This suggests that the binding energy of D_2 on the (100) steps of Pt(211) and Pt(533) are very similar. The maximum desorption rates for the (111) terraces shows larger differences. On Pt(211) it appears 11 K higher than for Pt(533) and the width of the desorption peaks broaden for the latter by more than a factor of two. These differences suggest that D atoms have, on average, a higher binding energy on the three-atom wide (111) terraces of Pt(211) than the four-atom wide (111) terraces of Pt(533) and that the wider terrace shows more variation in binding energy. These conclusions are fully in line with recent calculation for the binding energy variation of H to such surfaces. For both Pt(211)[44] and Pt(533)[45] binding energies were calculated and found to be highest for H atoms bound to the (100) step edge. When moving away from the bottom steps toward the next downward step along the terrace, the binding energy in the step edge and on three-fold hollow sites on the terrace progressively drop toward the value found for Pt(111).

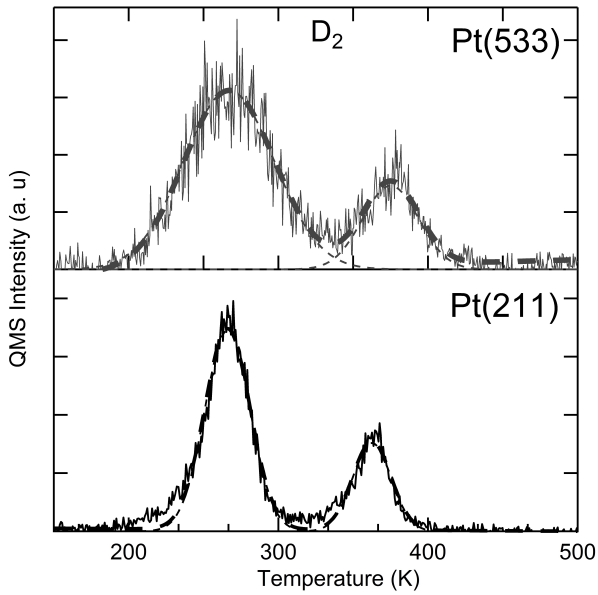

Figure 4.6: Comparison of D_2 TPD spectra for (top) Pt(533) and (bottom) (211) for maximum surface coverage.

We have also studied the effect of the terrace length on the ratio of terrace desorption to step desorption for deuterium on Pt[n(111)(100)] for $n = 3$, 4 and

6. Using fits as exemplified in figure 4.6, we find the ratio of terrace-bound D to step-bound D for n = 6, n = 4 and n = 3 to be 5.2, 3.1 and 2.7, respectively. As expected, for Pt[4(111)(100)] and Pt[6(111)(100)], the ratio of terrace-bound to step-bound D ratio is nearly proportional to *(n-1)*. For Pt[2(111)(100)] this ratio is markedly higher than what is predicted for $n = 3$. Again, we find a clear deviation from expected behavior which is also well beyond our uncertainty limits when n drops below 4.

4.4.3 Oxygen

In figure 4.7 we show TPD spectra for associative O_2 desorption from the maximum coverage created by dissociation of O_2 from background dosing for Pt(533) and Pt(211) in the top and bottom panels, respectively. The solid lines show our experimental data while the dashed lines are fits using Gaussian functions. Again, these are only used for integration purposes and do not represent physical processes. In order to compare relative sizes of TPD peaks, the fit to the high temperature peak for Pt(211) used the parameters for the width and central temperature determined for the same peak in the Pt(533) data[16]. Briefly, Pt(533) gives rise to two easily identifiable desorption peaks in the TPD spectrum between 550 and 900 K. The low temperature peak at 663 K results from associative desorption from (111) terrace sites. The desorption feature at 774 K strongly resembles high temperature desorption from other stepped Pt surfaces and is not present when using Pt(111)[46–49]. Hence, it is attributed to associative desorption from O atoms bound to (100) step sites. Comparison to theoretical calculations suggest that this is bridge-bonded oxygen at the (100) steps with every second bridge site being occupied[45, 50, 51].

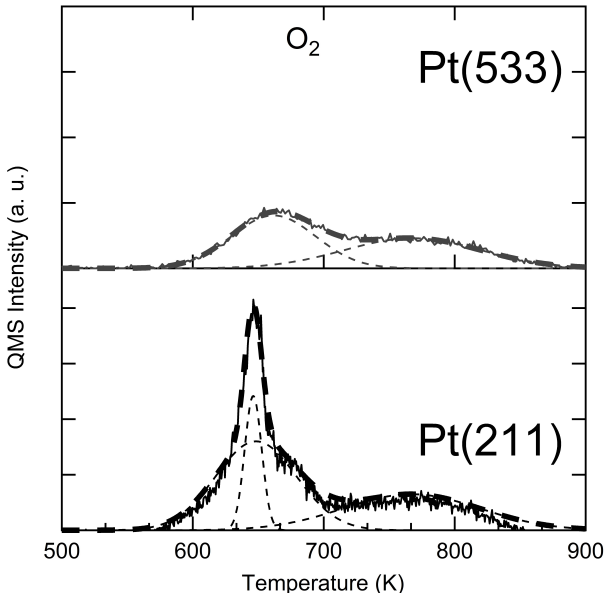

Figure 4.7: Comparison of O_2 TPD spectra for (top) Pt(533) and (bottom) (211) for maximum surface coverage. O_2 was dosed at Ts $\sim$ 100 K.

In the TPD trace for maximum coverage in bottom panel of figure 4.7, Pt(211) shows three desorption features. These are more easily identified in TPD traces appearing in figure 4.8 for varying initial coverages. There, we also separately show the regimes where O_2 desorbs from a molecularly adsorbed state between 100 and 200 K and the associative desorption occurring at much higher temperatures. At low initial coverage, a high temperature peak shows a maximum desorption rate at $\sim$780 K which strongly resembles the high temperature desorption feature for Pt(533)[16]. After saturation of the peak at highest temperature, a shoulder develops that turns into a distinct maximum at 677 K. Even higher initial doses lead to the third desorption peak that saturates with a maximum desorption rate at 646 K. This peak is considerably narrower than the former two peaks. The leading edge initiates at 570 K and shows unexpected behavior of zeroth-order desorption kinetics. The comparison between the peak shapes in figure 4.7 clearly shows that, again, there is a pronounced effect to this minor variation of terrace width from $n = 3$ to 4.

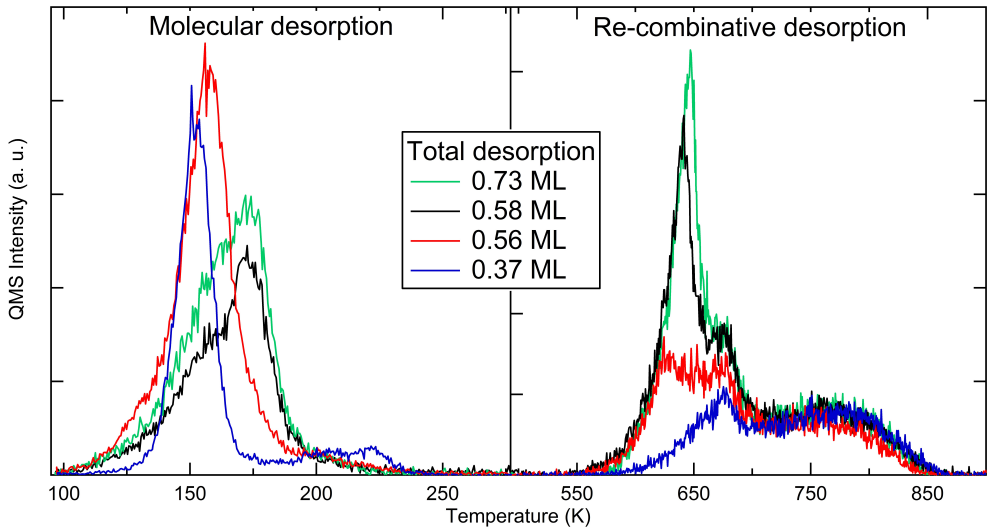

Figure 4.8: TPD spectra of varying amounts of O_2 desorbing from Pt(211). The low temperature panel (left) shows desorption of molecularly adsorbed O_2; high temperature panel (right) shows recombinative desorption of O_{ad}.

Our series of TPD spectra shown in figure 4.8 match those of a previous study on O_2 desorption from Pt(211) by Winkler et al.[52]. Although they also observed the sharp peak with overlapping leading edges and a well-defined shoulder between 650 and 700 K, they provided no suggestion for the origin of these two peaks appearing in the regime where O_2 is known to desorb from Pt(111). In a more recent study that used Pt(533) and O_2 adsorption from background dosing, the same single desorption feature in the temperature regime between 550 and 700 K was found that we report for Pt(533) in figure 4.7[16]. When using a supersonic molecular beam to dissociate O_2 on Pt(533), Gee and Hayden found a similar but considerably smaller third desorption peak in the same temperature regime. They attributed it to associative desorption of an atomic state due to the dissociation of O_2 at (100) steps[25]. Following the previous suggestions that a maximum coverage of 0.25 ML is obtained by background dosing on Pt(533) and a ratio of $O_{ads,step}$:$O_{ads,ter}$ of approximately 0.11:0.14[16, 25], we estimated the amounts of O contribution to the three desorption peaks observed for Pt(211). Here, we assume that the higher step density of Pt(211) also yields a proportionally higher total desorption from (100) steps around 750 K. We obtain a coverage of 0.15 ML for the desorption of bridge-bonded oxygen at the step and 0.29 ML for the combined lower temperature desorption. Pt(211) thus yields a maximum total O_{ads} coverage of 0.44 ML. We have analyzed the O-covered surface in detail by

LEED but find no evidence for an ordered overlayer structure.

To shed light on the origin of the more complex desorption and higher apparent O_{ads} coverage for the (211) surface, we consider other (TPD) studies that have focused on Pt oxidation and show a similar characteristic sharp feature at the lower side of the well-known recombinative desorption features. For Pt(553) (or Pt[(4(111)x(110)]), we have previously reported a similar sharp feature in desorption studies that only appeared when the surface was not properly annealed in between exposures and temperature ramps[15] . When plotting the highest obtained coverage for Pt(211) and Pt(553) in a single graph, these sharp peaks overlap nearly perfectly (not shown here). For the (332) surface (Pt[5(111)x(110)], which is very similar to Pt(533), Wang et al. have previously shown by a combined core-level spectroscopy and DFT study that an increased O-surface coverage resulted in 1-dimensional (1D) PtO_2 chains forming at these steps[53, 54]. A similar PtO_2 chain structure had also been suggested by a combined STM-DFT study for the top ridge of the reconstructed Pt(110)-(1x2) surface[55]. Note that the step edge for Pt(553), Pt(332) and this reconstructed (110) surface consist of the exact same spatial arrangement of the Pt atoms forming the edge. It is a triangular arrangement on either side of the lowest coordinated Pt atoms. On the basis of XPS, TPD, STM and DFT studies, Weaver and coworkers came to the conclusion that similar 1-D PtO_2 chains can even be produced on Pt(111) using an atomic oxygen source. The 1-D PtO_2 chains directly relate to the sharp β_1 desorption feature in their TPD spectra[56–59]. A similar TPD feature was much earlier observed for high O-coverages on Pt(111) produced from NO_2 dissociation[60] and also appears for the hexagonally reconstructed Pt(100) surface[61]. A study by Gland on Pt(111) and Pt[11(111)x(110)] did not reveal the sharp recombinative desorption feature for the stepped surface, although the additional molecular desorption feature that appears characteristic for steps was present[46, 47].

Considering these previous results, the appearance of the sharp feature in our TPD traces for Pt(211) between 600 and 650 K may be interpreted to suggest that the (100) step edge on Pt(211) is capable of producing 1D-chains of PtO_2. This is remarkable as the Pt(533) surface with the same (100) step type has no or very little tendency to do so. Only at high incident energy, the onset of this characteristic desorption feature is observed in TPD experiments following adsorption from a supersonic molecular beam[62]. Wang et al. did not find this peak using background dosing onto Pt(533)[63]. We also do not observe it for Pt(533), even after high exposures at room temperature. Hence, if this TPD peak for Pt(211) is indeed related to the formation of 1D-PtO_2 chains at higher O_2 exposures, the ease with which the feature appears in our study suggests that the barrier to O_2 dissociation leading to a coverage beyond 0.25 ML critically

depends on terrace width and changes between $n = 3$ and $n = 4$.

We scrutinize our TPD results in figure 4.8 to obtain a better view of the requirement to obtain the desorption feature that resembles desorption from 1-D PtO_2 chains. At a total desorption equivalent to 0.37 ML O (blue) we identify one major and two small features for desorption from molecular states at 153 K, 202 K and 222 K. Following the interpretation by Wintterlin et al. for Pt(111), we attribute the feature at 153 K to desorption of O_2 bound in molecular clusters to (111) terrace sites[64]. During desorption of O_2 molecules, other O_2 molecules dissociate as the barriers for these processes are similar. Desorption at slightly higher temperatures (between 200 and 250 K) may be due to O_2 adsorbed to bare (100) steps. At the initial dose leading to a total desorption of 0.37 ML, we find predominantly recombinative desorption from regular step-bound O_{ads}. These atoms may have dissociated at terrace sites and diffused to step sites during the temperature ramp, but may also have dissociated at the step. At 0.56 ML total O coverage (red), the main molecular desorption peak broadens and shifts to 157 K. In the recombinative desorption regime, the lower temperature desorption peak at 626 K has appeared. Increasing the initial dose further to 0.58 total O_{ads} coverage (black), the desorption of molecularly bound O_2 suddenly changes. The lowest desorption peak drops in intensity and a peak at 172 K dominates. In the right panel, the sharp feature with apparent zeroth-order desorption kinetics grows in rapidly. For 0.73 ML total O coverage (green), even more O_2 desorbs from molecular states, while the recombinative desorption saturates.

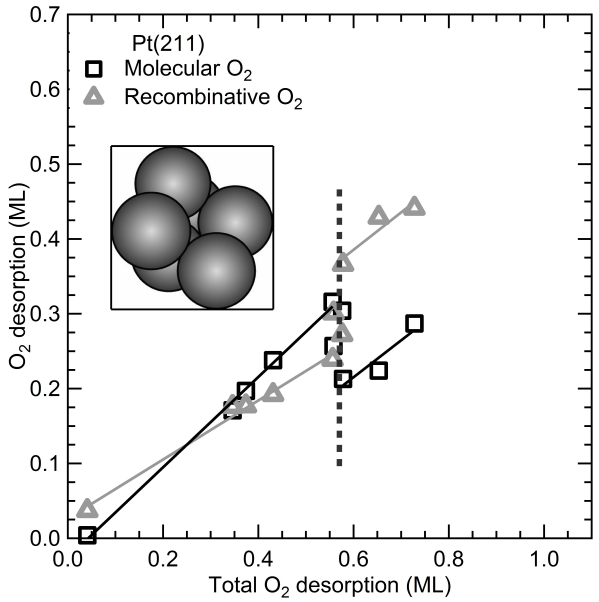

Figure 4.9: Integrated O_2 TPD signals for molecular and recombinative desorption as a function on initial O_2 coverage on Pt(211). The dotted-vertical line indicates the critical coverage near 0.56 ML.

To clarify the sudden change around a total desorption near 0.56 ML, we separately quantify in figure 4.9 the observed molecular and recombinative O_2 desorption as a function of total O_2 desorption. Both show a linear dependence before and after 0.56 ML, however the partitioning between molecular and recombinative desorption drastically changes above this coverage. From competing desorption and dissociation during the initial stages of the temperature ramp, the latter benefits from high initial O_2 coverages. For Pt(111), Miller et al. showed that attractive adsorbate-adsorbate interactions affect the dissociation of O_2[65]. In particular, they found that the desorption energy increased while the dissociation energy decreased for the molecular coverage regime of 0 - 0.25 ML O_2. This is to be compared to 0 - 0.50 ML O_{ads} coverage in our figure 4.9. Our results show that partitioning between desorption and dissociation below 0.56 ML for Pt(211) is not strongly affected by the initial coverage over this range as both components show nearly identical changes with initial coverage. If lateral interactions affect the partitioning in this regime, it actually favors desorption in contrast to what Miller et al. suggest for Pt(111). However, we observe for the stepped surface a sudden increase in the dissociation relative to desorption at ∼0.56 ML O (or 0.28 ML O_2), whereas for Pt(111) the opposite trend was predicted. There, the barrier

to dissociation increased from 0.24 eV to 0.74 eV between O_2 adsorbate structures representing a total of 0.5 and 1.0 ML O. Hence, the (100) step introduces an additional effect in providing an alternative site or pathway for dissociation with an additional lowering of the activation barrier. At 0.56 ML total initial O, a turning point is reached above which desorption from the molecular state is reduced. It leads to an upward temperature shift in the molecular desorption regime and a rapid growth of the feature that resembles the feature observed for 1-D PtO_2 chains.

If PtO_2 chains form at the step edge during the temperature ramp, it must stoichiometrically be reflected in the TPD traces. Considering the development of the three associative desorption peaks in our TPD spectra, the previously mentioned ratio of 0.15:0.29 for the single high and two combined lower temperature peaks are more likely to represent an approximate ratio of 1:1:1 for three types of O atoms desorbing from to step, terrace, and step sites. As at lower total coverages oxygen binds at the step with only one O atom per 2 Pt atoms (every second bridge site), this makes the Pt:O stoichiometry for the highest obtained coverage in our spectra 1:1 and not 1:2 for Pt_{step}:O. For an ordered overlayer forming PtO at the step and an O-atom bound to a three-fold site at the terrace, the ultimate coverage would become 0.50 ML, whereas we find a maximum of 0.44 ML. Not reaching the highest coverage is reasonable that the atomically-bound oxygen is formed from dissociation of molecularly-bound O_2 that may also desorb in a parallel process. It is also supported by the lack of long-range order for an overlayer in LEED patterns.

We finally speculate on the origin of the different tendencies to form the high coverage structure, along the step for $n = 3$ and $n = 4$. First, we recall that the (100) step type has a triangular arrangement of Pt atoms on one side and a square arrangement on the other side. For the (100) and (110) step types, other adsorption sites for O are preferred in the low coverage regime[45, 50]. For the (110) step type, oxygen atoms adsorb preferentially in the three-fold hollow on the upper terrace, whereas for the (100) step the bridge site is preferred. Molecular O_2 adsorption occurs prior to dissociation with the O-O bond parallel to the step edge[51, 66, 67]. The differences in TPD traces for stepped surfaces and the (111) plane suggest that the O_2 dissociation and desorption occurs at the terrace prior to the step ($\sim$150 K vs. 220-250 K). The difference between Pt(211) and Pt(533) in producing the additional sharp TPD features thus seems related to the initial O_2 dissociation and the exact sites where oxygen atoms adsorb on the narrow (111) plane. Apparently, for the 3-atom wide terrace with a (100) step, this occurs such that it alters subsequent dissociation/desorption at the step. It leads to more facile dissociation and to a desorption feature that we attribute to

PtO-like chains at the step.

We note that TPD results can be misleading with regards to stoichiometry and desorption sites. For example, in a previous combined theoretical and experimental study we showed that three peaks in the desorption of H_2 from Pt(110)(1x2) are not a consequence of three different desorption sites[68]. Hence to confirm the proposed stoichiometry, other techniques are needed. figure 4.10 shows two schematics of potential surface structures for ordered overlayers of atomic oxygen on Pt(533) and Pt(211) that would explain the similarity in TPD structures for O coverages well below the maximum coverage and the ratios of integrated TPD peaks. It assumes a maximum coverage of 0.25 ML for Pt(533)[62] and suggests a true maximum coverage of 0.50 ML for O/Pt(211). On Pt(533), the strongest adsorption site on the terrace is the FCC hollow[45], which is the first atomic oxygen to be created during the temperature ramp when other terrace-bound O_2 desorbs. Consecutive O_2 desorption from step sites creates space for additional dissociative adsorption at the (100) steps. The narrower terrace of Pt(211), leads to HCP-bound O instead of FCC-bound O if the step edges again are also covered by O_2. We suggest that this may drive the higher level of consecutive O_2 dissociation at the step during the temperature ramp for Pt(211) leading to a ratio of 1:1 for Pt_{step}:O.

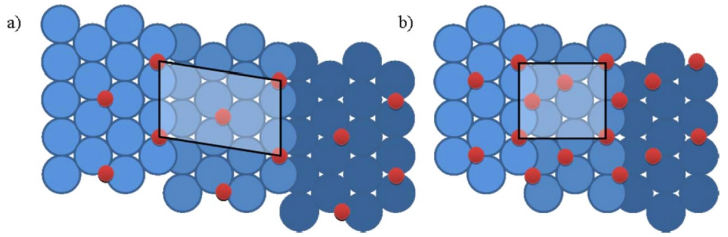

Figure 4.10: Idealized adsorbate structures for a) O/Pt(533) with a 1:1 O_{step}:$O_{terrace}$ ratio and 0.25 ML and b) O/Pt(211) representing, a 2:1 O_{step}:$O_{terrace}$ ratio and 0.50 ML.

4.5 Conclusions

In this study we have shown that surfaces having the same step type and terrace geometries may show very different behaviors even for changes in terrace width of only one atom. For D_2, recombinative desorption from the step edge seems not affected by the width of the neighboring terraces. This is in line with our previous molecular beam adsorption studies, where we found that the reactivity on Pt(211) may be used to quantitatively predict the reactivity for all other surfaces of the

same type in the zero-coverage limit[10, 69]. However, the presence of the step affects the binding energy for H atoms on the terrace mostly close to the step edge. We observe this effect in recombinative desorption. A narrow terrace only contains sites that are all affected by the step, whereas a wider terrace contains sites more strongly resembling the infinite (111) plane. Hence, the wider the terrace, the larger the variation in binding energy and the broader the desorption feature from terrace sites. For water adsorption to Pt(211), we find crystalline growth at temperatures where on Pt(533) and surfaces with even wider terrace ASW forms. Here, the surface structure steers adsorption and affects mobility of molecules such that it enhances lateral ordering of adsorbates on (211). We expect that this is a consequence of the distance between step edges where water generally tends to accumulate. The crystallinity of water and exact structure may be confirmed and further investigated experimentally by, e.g., STM and RAIRS studies, or by theory. Finally, O_2 dissociation is also affected by terrace width. We find a considerably larger O coverage on this surface resulting from enhanced dissociation of molecularly adsorbed O_2 at high initial coverage. A simple quantitative analysis of our TPD results shows that we likely form a stoichiometric ratio of 1:1 for Pt_{step}:O.

Our results thus give reason to be cautious in extrapolating results from theoretical studies on the smallest unit cell to larger structures. For H_2, the lowering of the dissociation barrier locally at the step is probably not affected by terrace length. However, the effect that the step has on binding sites near the step is strong close to the step and weakens with distance. Hence the potential influence of the step to altering diffusion, reaction and desorption at the terrace is dependent on terrace length. We observe these effects directly in our TPD experiments and see different behavior already when comparing 3 and 4 atom wide terraces. This obviously also directly relates to overall kinetics of chemical reaction as with increasing particle diameter the terrace size increases and ratio of step-to-terrace sites drops. For O_2 dissociation, we suggest that the exact location of O atoms formed at the terrace influences consecutive dissociation at the step. Here, the barrier to dissociation at the step is affected by the terrace length, but only through the location of the terrace-bound O atom. Finally, for H_2O adsorption, the delicate balance between lateral interactions and individual binding energies seems not allow for any extrapolation from studies using a single small unit cell.

4.6 Bibliography

References

(1) Reith, F; Campbell, S. G.; Ball, A. S.; Pring, A; Southam, G English *Earth-Science Reviews* **2014**, *131*, 1–21.

(2) Wang, H.; An, K.; Sapi, A.; Liu, F.; Somorjai, G. A. *Catalysis Letters* **2014**, *144*, 1930–1938.

(3) Thiel, P. A.; Madey, T. E. *Surface Science Reports* **1987**, *7*, 211–385.

(4) Ranke, W *Surface Science* **1989**, *209*, 57–76.

(5) Matsushima, T. *Surface Science* **1985**, *157*, 297–318.

(6) Rettner, C. T.; Mullins, C. B. English *Journal of Chemical Physics* **1991**, *94*, 1626–1635.

(7) Christmann, K; Ertl, G; Pignet, T *Surface Science* **1976**, *54*, 365–392.

(8) Bădescu, Ş.; Salo, P.; Ala-Nissila, T; Ying, S.-C.; Jacobi, K.; Wang, Y.; Bedürftig, K.; Ertl, G. *Physical review letters* **2002**, *88*, 136101.

(9) Luntz, A. C.; Brown, J. K.; Williams, M. D. *Journal of Chemical Physics* **1990**, *93*, 5240–5246.

(10) Groot, I. M. N.; Kleyn, A. W.; Juurlink, L. B. F. *Angewandte Chemie-International Edition* **2011**, *50*, 5174–5177.

(11) Luntz, A. C.; Grimblot, J; Fowler, D. E. *Physical Review B* **1989**, *39*, 12903–12906.

(12) Luntz, A. C.; Williams, M. D.; Bethune, D. S. *Journal of Chemical Physics* **1988**, *89*, 4381–4396.

(13) Derry, G. N.; Ross, P. N. *Surface Science* **1984**, *140*, 165–180.

(14) Hodgson, A.; Haq, S. *Surface Science Reports* **2009**, *64*, 381–451.

(15) Van der Niet, M. J. T. C.; den Dunnen, A.; Juurlink, L. B. F.; Koper, M. T. M. *Physical Chemistry Chemical Physics* **2011**, *13*, 1629–1638.

(16) Van der Niet, M. J. T. C.; den Dunnen, A.; Juurlink, L. B. F.; Koper, M. T. M. *Journal of Chemical Physics* **2010**, *132*, 174705–174713.

(17) Vanhove, M. A.; Somorjai, G. A. *Surface Science* **1980**, *92*, 489–518.

(18) Watwe, R. M.; Cortright, R. D.; Norskov, J. K.; Dumesic, J. A. *Journal of Physical Chemistry B* **2000**, *104*, 2299–2310.

(19) Greeley, J; Rossmeisl, J; Hellman, A; Norskov, J. K. English *Zeitschrift Fur Physikalische Chemie-International Journal of Research in Physical Chemistry & Chemical Physics* **2007**, *221*, 1209–1220.

(20) Peterson, A. A.; Grabow, L. C.; Brennan, T. P.; Shong, B.; Ooi, C.; Wu, D. M.; Li, C. W.; Kushwaha, A.; Medford, A. J.; Mbuga, F.; Li, L.; Norskov, J. K. *Topics in Catalysis* **2012**, *55*, 1276–1282.

(21) Janlamool, J.; Bashlakov, D.; Berg, O.; Praserthdam, P.; Jongsomjit, B.; Juurlink, L. B. F. *Molecules* **2014**, *19*, 10845–10862.

(22) Van Reijzen, M. E.; van Spronsen, M. A.; Docter, J. C.; Juurlink, L. B. F. *Surface Science* **2011**, *605*, 1726–1731.

(23) Yates Jr, J. T. *Springer, New York* **1998**, *27*, 181–0013.

(24) Den Dunnen, A.; van der Niet, M. J. T. C.; Koper, M. T. M.; Juurlink, L. B. F. *Journal of Physical Chemistry C* **2012**, *116*, 18706–18712.

(25) Gee, A. T.; Hayden, B. E.; Mormiche, C; Nunney, T. S. English *Journal of Chemical Physics* **2000**, *112*, 7660–7668.

(26) Nieskens, D.; van Bavel, A.; Niemantsverdriet, J. *Surface Science* **2003**, *546*, 159–169.

(27) Habenschaden, E; Kuppers, J *Surface Science* **1984**, *138*, 147–150.

(28) Tait, S. L.; Dohnalek, Z; Campbell, C. T.; Kay, B. D. *Journal of Chemical Physics* **2005**, *122*.

(29) Den Dunnen, A.; van der Niet, M. J. T. C.; Badan, C.; Koper, M. T. M.; Juurlink, L. B. F. *Physical Chemistry Chemical Physics* **2014**, 8530–8537.

(30) Petrik, N. G.; Kimmel, G. A. English *Journal of Chemical Physics* **2004**, *121*, 3736–3744.

(31) Speedy, R. J.; Debenedetti, P. G.; Smith, R. S.; Huang, C; Kay, B. D. *Journal of Chemical Physics* **1996**, *105*, 240–244.

(32) Dohnalek, Z; Ciolli, R. L.; Kimmel, G. A.; Stevenson, K. P.; Smith, R. S.; Kay, B. D. English *Journal of Chemical Physics* **1999**, *110*, 5489–5492.

(33) Van der Niet, M. J. T. C.; Dominicus, I.; Koper, M. T. M.; Juurlink, L. B. F. *Physical Chemistry Chemical Physics* **2008**, *10*, 7169–7179.

(34) Smith, R. S.; Matthiesen, J.; Knox, J.; Kay, B. D. *Journal of Physical Chemistry A* **2011**, *115*, 5908–5917.

(35) Kimmel, G. A.; Petrik, N. G.; Dohnalek, Z; Kay, B. D. *Physical Review Letters* **2005**, *95*, 166102–166106.

(36) Kimmel, G. A.; Petrik, N. G.; Dohnalek, Z.; Kay, B. D. *Journal of Chemical Physics* **2006**, *125*, 44713–44725.

(37) Kimmel, G. A.; Petrik, N. G.; Dohnalek, Z.; Kay, B. D. *Journal of Chemical Physics* **2007**, *126*, 114702–114712.

(38) Endo, O.; Nakamura, M.; Sumii, R.; Amemiya, K. *Journal of Physical Chemistry C* **2012**, *116*, 13980–13984.

(39) Nakamura, M.; Sato, N.; Hoshi, N.; Soon, J. M.; Sakata, O. *Journal of Physical Chemistry C* **2009**, *113*, 4538–4542.

(40) Fajín, J. L. C.; D. S. Cordeiro, M. N.; Gomes, J. R. B. *The Journal of Physical Chemistry A* **2014**, *118*, 5832–5840.

(41) Donadio, D.; Ghiringhelli, L. M.; Delle Site, L. *Journal of the American Chemical Society* **2012**, *134*, 19217–19222.

(42) Collins, D. M.; Spicer, W. E. *Surface Science* **1977**, *69*, 85–113.

(43) Lu, K. E.; Rye, R. R. *Surface Science* **1974**, *45*, 677–695.

(44) Olsen, R. A.; Kroes, G. J.; Baerends, E. J. *Journal of Chemical Physics* **1999**, *111*, 11155–11163.

(45) Kolb, M. J.; Calle-Vallejo, F.; Juurlink, L. B. F.; Koper, M. T. M. *The Journal of chemical physics* **2014**, *140*, 134708.

(46) Gland, J. L.; Sexton, B. A.; Fisher, G. B. *Surface Science* **1980**, *95*, 587–602.

(47) Gland, J. L.; Sexton, B. A.; Fisher, G. B. *Surface Science* **1980**, *95*, 587–602.

(48) Steininger, H; Lehwald, S; Ibach, H *Surface Science* **1982**, *123*, 1–17.

(49) Avery, N. R. *Chemical Physics Letters* **1983**, *96*, 371–373.

(50) Gambardella, P; Sljivancanin, Z; Hammer, B; Blanc, M; Kuhnke, K; Kern, K *Physical Review Letters* **2001**, *87*.

(51) Šljivančanin, Z.; Hammer, B. *Surface Science* **2002**, *515*, 235–244.

(52) Winkler, A.; Guo, X.; Siddiqui, H. R.; Hagans, P.; Yates, J. T. *Surface Science* **1988**, *201*, 419–443.

(53) Wang, J. G.; Li, W. X.; Borg, M.; Gustafson, J.; Mikkelsen, a.; Pedersen, T. M.; Lundgren, E.; Weissenrieder, J.; Klikovits, J.; Schmid, M.; Hammer, B.; Andersen, J. N. *Physical Review Letters* **2005**, *95*, 1–4.

(54) Ogawa, T.; Kuwabara, A.; Fisher, C. A. J.; Moriwake, H.; Miwa, T. *Journal of Physical Chemistry C* **2013**, *117*, 9772–9778.

(55) Helveg, S; Lorensen, H. T.; Horch, S; Laegsgaard, E; Stensgaard, I; Jacobsen, K. W.; Norskow, J. K.; Besenbacher, F *Surface Science* **1999**, *430*, 533–539.

(56) Hawkins, J. M.; Weaver, J. F.; Asthagiri, A. *Physical Review B* **2009**, *79*, 125434.

(57) Devarajan, S. P.; Hinojosa Jr., J. A.; Weaver, J. F. *Surface Science* **2008**, *602*, 3116–3124.

(58) Weaver, J. F.; Chen, J. J.; Gerrard, A. L. *Surface Science* **2005**, *592*, 83–103.

(59) Weaver, J. F.; Kan, H. H.; Shumbera, R. B. *Journal of Physics-Condensed Matter* **2008**, *20*.

(60) Parker, D. H.; Bartram, M. E.; Koel, B. E. *Surface Science* **1989**, *217*, 489–510.

(61) Shumbera, R. B.; Kan, H. H.; Weaver, J. F. English *Surface Science* **2007**, *601*, 4809–4816.

(62) Gee, A. T.; Hayden, B. E. *The Journal of Chemical Physics* **2000**, *113*, 10333–10343.

(63) Wang, H; Tobin, R. G.; Lambert, D. K.; DiMaggio, C. L.; Fisher, G. B. *Surface Science* **1997**, *372*, 267–278.

(64) Wintterlin, J; Schuster, R; Ertl, G English *Physical Review Letters* **1996**, *77*, 123–126.

(65) Miller, D. J.; Oberg, H; Naslund, L. A.; Anniyev, T; Ogasawara, H; Pettersson, L. G. M.; Nilsson, A English *Journal of Chemical Physics* **2010**, *133*, 224701–224707.

(66) Sano, M; Ohno, Y; Yamanaka, T; Matsushima, T; Quinay, E.; Jacobi, K *The Journal of chemical physics* **1998**, *108*, 10231–10238.

(67) Yamanaka, T; Matsushima, T; Tanaka, S; Kamada, M English *Surface Science* **1996**, *349*, 119–128.

(68) Gudmundsdottir, S.; Skulason, E.; Weststrate, K.-J.; Juurlink, L.; Jonsson, H. *Physical Chemistry Chemical Physics* **2013**, *15*, 6323–6332.

(69) Groot, I. M. N.; Kleyn, A. W.; Juurlink, L. B. F. *Journal of Physical Chemistry C* **2013**, *117*, 9266–9274.